Polymer 49 (2008) 2119–2126

Contents lists available at ScienceDirect

Polymer

journal homepage: www.elsevier.com/locate/polymer

Structural analysis of multicomponent nanoclay-containing polymer blends through simple model systems

Ladan As'habi [a], Seyed Hassan Jafari [a,*], Bahareh Baghaei [a], Hossein Ali Khonakdar [b], Petra Pötschke [c], Frank Böhme [c]

[a] School of Chemical Engineering, University of Tehran, P.O. Box 11155-4563, Tehran, Islamic Republic of Iran
[b] Iran Polymer and Petrochemical Institute, P.O. Box 14965/115, Tehran, Islamic Republic of Iran
[c] Leibniz Institute of Polymer Research Dresden, Hohe Strasse 6, D-01069, Dresden, Germany

ARTICLE INFO

Article history:
Received 2 October 2007
Received in revised form 5 February 2008
Accepted 25 February 2008
Available online 6 March 2008

Keywords:
Polymer nanocomposite
Polymer blend
Organoclay

ABSTRACT

A systematic approach was adopted to study multicomponent clay-containing nanocomposites using compatibilized and non-compatibilized blends of polyamide 6 (PA6)/acrylonitrile–butadiene–styrene terpolymer (ABS) and their organoclay (OMMT) nanocomposites. For this purpose PA6/styrene–acrylonitrile copolymer (SAN) based blends and nanocomposites were selected as simple model systems. In this way the role of each component of the systems, especially the clay, compatibilizer, and polybutadiene fraction on the formation of intercalated or exfoliated OMMT structures as well as resulting dynamic mechanical properties (DMA) could be elucidated. Structural analysis of the model systems using theoretical approach, and X-ray diffraction, transmission electron microscopy, scanning electron microscopy, and DMA revealed that the most crucial factor in controlling the morphology and achieving different levels of dispersion is the extent of interaction between clay and the polymer matrix. Morphological analysis revealed that the OMMT layers were dispersed and exfoliated largely in the PA6 phase but, some were also accumulated at the rubber particle surface which remained non-intercalated. The effect of a compatibilizer on the dispersion of OMMT was not completely clear. The SAN based nanocomposites containing PA6 showed fully exfoliated OMMT structures, whereas the ABS based nanocomposites, having an additional rubber fraction, showed a mixed exfoliated and also partly non-intercalated morphology. The OMMT did not change the general occurrence of the co-continuous structures but refined the structures and led to mechanical stiffening as indicated by the DMA results. A correlation was established between the changes in the morphological states and the DMA properties.

1. Introduction

Fillers play an important role in modifying the desirable properties of polymers and reducing the cost of their composites. It is logical to anticipate that the dispersion of fillers with dimensions in the nanometer level having very large aspect ratio and stiffness in a polymer matrix could lead to even higher mechanical performances [1–3]. These fillers mainly include layered silicates and carbon nanotubes. Polymer nanocomposites, especially polymer/clay nanocomposites have been of great commercial interest since the past decade. The greatest improvement comes with exfoliated samples, with the exception of flammability properties, where both intercalated and exfoliation materials seem to have the same influence. Although many polymers have been used to prepare nanocomposites with layered silicates, little work has been carried out on nanocomposites based on polymer blend systems [4–11]. It is thought that polymer blend nanocomposites may lead to a new kind of high performance material, which combines the advantages of polymer blends and the merits of polymer nanocomposites.

Wang and coworkers showed that the polystyrene (PS) domain size is greatly decreased upon the addition of organoclay (OMMT) in the PS/polypropylene (PP) system. They attributed this phenomenon to the fact that two immiscible polymer chains can exist together between the intercalated clay platelets; thus these two chains play the role of a block copolymer [4]. On the other hand, Khatua and coworkers investigated polyamide 6 (PA6)/ethylene–propylene rubber (EPR) blend nanocomposite and found that the domain size of EPR phase in the PA6 matrix decreased significantly even when only a small amount of OMMT was added [5]. They explained this behavior in terms of preventing coalescence of the dispersed domains by the exfoliated clay platelets. Lee and Shimizu

* Corresponding author. Tel.: +98 21 61112857; fax: +98 21 66957784.
E-mail address: shjafari@ut.ac.ir (S.H. Jafari).

0032-3861/$ – see front matter © 2008 Elsevier Ltd. All rights reserved.
doi:10.1016/j.polymer.2008.02.049

investigated the morphology of polyphenylene oxide (PPO)/PA6 blend nanocomposites with various amounts of clay. It was found that the selective localization of exfoliated clay platelets in the PA6 phase not only increased the viscosity of PA6 and changed the viscosity ratio of the PA6 phase and the PPO phase, but also impeded the coalescence of the PPO phase [6]. Gelfer et al. found that the PS domain size in PS/polymethyl methacrylate (PMMA) blend was reduced upon adding OMMT because of the compatibilization function of the excessive surfactant in OMMT and increased viscosity [7]. Lim and coworkers reported similar findings on interaction characteristics of OMMT in a miscible polymer blend of polyethylene oxide and PMMA [9].

Multicomponent compatibilized blends based on PA6 with acrylonitrile–butadiene–styrene terpolymer (ABS) are well established commercial materials having a good combination of toughness, stiffness, and processability [12–19]. To further improve their stiffness for engineering applications in which high dimensional stability is a key point normally glass reinforced grades of these blends are used which sacrifice their ease of processability due to severe increase in viscosity [20]. Considering the role of nanoclays in enhancement of mechanical performances of polymers, it is expected that the addition of small amount of nanoclays to the PA6/ABS blend system improve its mechanical and thermal properties as well as its flame retardant behavior without hampering its processability. In this context some reports about PA6/ABS blend-based nanocomposites have been published recently. These reports mainly focused on the study of thermal and impact properties of PA6/clay nanocomposites blended with ABS [21,22], dynamic mechanical properties [23], effect of microcompounding process parameters on properties of ABS/PA6 blends filled with OMMT [24,25], fractionated crystallization and electrical conductivity of carbon-nanotube filled PA6/ABS nanocomposites [26,27]. However, there were difficulties with study of such system in terms of understanding the mechanism for an effective dispersion process and its effect on the resulting properties since the PA6/ABS blend nanocomposite is an intricate multicomponent system in which each component can play a major role in dictating the final state of dispersion of the nano-scale fillers. Hence, there is a necessity for a systematic study of such nanocomposite blend systems using a series of simple model systems. Styrene acrylonitrile copolymer (SAN) based blends and nanocomposites can be a suitable choice for acting as model systems. Studies on these simple blends and nanocomposites provide a basis for a better understanding of the structure–properties correlation in multicomponent PA6/ABS blend nanocomposites.

2. Experimental

2.1. Materials and sample preparation

All the materials [PA6 Durethan B29, SAN Lustran M60, ABS Novodur Graft (SAN-*g*-PB), and SANMA], supplied by Bayer AG, Dormagen, Germany, were in pellet form except for SAN-*g*-PB, which was delivered in a powder form. The organoclay (OMMT) employed in this work was Nanofil 2 (Süd-Chemie, Industry Group Plastic Additives). Nanofil 2 is a montmorillonite organically modified with stearylbenzyldimethyl-ammonium chloride in order to increase the gallery spacing of the original Na^+-montmorillonite. Before mixing, all the polymers and the OMMT were dried in a vacuum oven at 80 °C for 12 h.

The blends and nanocomposites were prepared via a one step process in a DACA conical twin screw microcompounder. Prior to the melt mixing process all the components of the blends or nanocomposites, in a specified ratio, were dry premixed and then fed into the microcompounder. The SAN and ABS based nanocomposites and blends were prepared with an identical composition keeping the PA6 content constant at 50 wt%. The compatibilized blends and nanocomposites had about 5 wt% SANMA. The OMMT loading in each nanocomposite sample was about 5 wt% of the total mixture. In addition, the neat components (PA6, SAN, SANMA and ABS polymers) were melt-mixed separately with 5 wt% OMMT under similar processing conditions. A processing temperature of 260 °C, a screw speed of 100 rpm, and a mixing time of 10 min were used for preparation of all the blends and nanocomposites. The extruded strands were cooled on an aluminum tray in air. For dynamic mechanical analysis (DMA) studies the extruded strands were compression molded into rectangular 0.5 mm thick sheets with dimensions of 20 mm × 10 mm. The molding was performed at a temperature of 260 °C and a pressure of 10 MPa.

2.2. Characterization

Wide-angle X-ray scattering (WAXS) patterns were recorded using Cu K_α radiation (40 kV, 30 mA) generated by an X-ray diffractometer (Xpert, Philips); corresponding data were collected from 2θ angle of 1.5° to 10° to characterize the spacing of the layer structure of the neat OMMT as well as that of the nanocomposite samples in the form of short strands. The scanning rate was 1°/min with a step size of 0.1°.

The dispersion of the OMMT platelets in the blend was studied by means of transmission electron microscopy (TEM). Ultra thin sections of the extruded samples (approximately 70 nm thick) were obtained at room temperature, using a Reichert OM-U3 ultramicrotome equipped with a diamond knife. The sections supported on 400-mesh grids were exposed to OsO_4 vapors in a desiccator containing 2 ml of 1% aqueous solution of OsO_4 for 30 min in order to stain SAN or ABS components of nanocomposites. The stained sections were observed by means of a PHILIPS CM200 FEG STEM, using an accelerated voltage of 200 kV.

Scanning electron microscopy (SEM) was used to characterize the morphology of the blends and nanocomposites. An extruded polymer strand was immersed in liquid nitrogen for some time and a brittle fracture was performed. The fractured surface was etched in formic acid for 2 h to remove the PA6 phase of the blends and nanocomposites. The etched surfaces after proper drying were gold sputtered and observed under a PHILIPS CM200.

Dynamic mechanical analysis was performed using a Triton DMTA in a bending mode using a single cantilever with a frequency of 10 Hz, a temperature range of −120°C to 200°C and a heating rate of 5 K/min on the compression molded samples with the dimension 20 mm × 10 mm × 0.5 mm. The deformation was about 0.05% and within the linear viscoelastic range.

3. Results and discussion

3.1. WAXS

For two-phase immiscible polymer blend/clay nanocomposites, such as PA6/ABS with OMMT, the properties of the nanocomposites greatly depend on the morphology of clay in the polymer blend matrices, so it is worth evaluating the dispersion of clay in polymer blend/clay nanocomposites.

Fig. 1 shows the X-ray diffraction (XRD) patterns of the OMMT and the nanocomposites of the neat components of the systems namely PA6, SAN, ABS and SANMA. All the nanocomposites contained 5% OMMT. As indicated in Fig. 1(e), the neat OMMT shows the (001) diffraction at $2\theta = 4.85°$. This peak corresponds to an interlayer spacing of 1.82 nm.

The strong diffraction peak is absent in the PA6 nanocomposite (Fig. 1(d)). This indicates that the OMMT platelets were completely exfoliated in the PA6 matrix. The polar nature of PA6 is responsible for this good level of interaction between OMMT and PA6 leading to

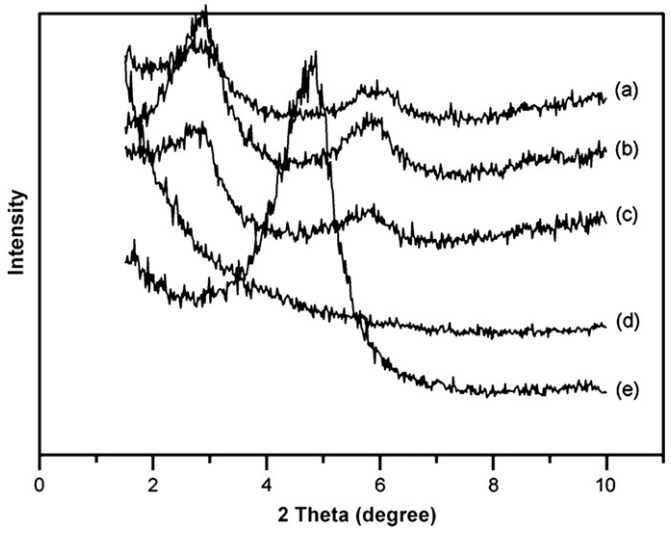

Fig. 1. XRD patterns of (a) SAN/5% OMMT; (b) SANMA/5% OMMT; (c) ABS/5% OMMT; (d) PA6/5% OMMT and (e) neat OMMT.

a fully exfoliated structure for PA6/OMMT nanocomposite. As it is seen from Fig. 1(a–c) all the three styrenic nanocomposites, namely SAN/OMMT, SANMA/OMMT and ABS/OMMT nanocomposites, show two X-ray diffraction peaks characteristic of unexfoliated structures. The XRD patterns were analyzed and the data corresponding to the gallery spacings ((d_{001})) are presented in Table 1.

As it is seen, the characteristic (001) peak of the OMMT for SAN nanocomposites shifted to $2\theta = 2.73^\circ$ corresponding to a d-spacing of 3.23 nm, which indicates that some SAN molecular chains were intercalated between the OMMT galleries, forming an intercalated structure. On the other hand, the d_{001} peaks of SANMA/5% OMMT and ABS/5% OMMT appear at 30.8 Å and 31.1 Å, respectively, indicating intercalated structures, too, but with slightly lower d-spacing as compared to the SAN/OMMT nanocomposite. However, the differences between the d-spacing values for all the styrenic based nanocomposites are relatively small and therefore they all should have similar intercalated structures. In other words the abilities of these three polymers to swell the OMMT crystallites are similar and the rubber particles in ABS/OMMT composites do not appear to affect the swelling process [28]. The XRD patterns presented in Fig. 1 lead one to assume that in presence of PA6, OMMT will be mainly localized in the PA6 phase of the blend-based nanocomposites. However, it is difficult for XRD to reveal definitive conclusions about the defined structure. Here, TEM is necessary to characterize the structure of the nanocomposites.

Fig. 2 shows XRD patterns of different blend-based nanocomposites. The SANMA component is assumed to act as a compatibilizer, stabilizing the blend structure. As it is seen, the XRD patterns for PA6/SAN/OMMT and PA6/SAN/SANMA/OMMT nanocomposites (Fig. 2(c and d)) are similar to the patterns obtained for the PA6/OMMT nanocomposite and no distinct diffraction peaks are seen.

Table 1
XRD data for the neat components, blends, and nanocomposites

Samples	2θ (°)	(d_{001}) (Å)
OMMT	4.85	18.2
PA6/5% OMMT	–	–
ABS/5% OMMT	2.84	31.1
SAN/5% OMMT	2.73	32.3
SANMA/5% OMMT	2.87	30.8
PA6/SAN/5% OMMT	–	–
PA6/ABS/5% OMMT	4.6	19.2
PA6/SAN/SANMA/5% OMMT	–	–
PA6/ABS/SANMA/3% OMMT	4.5	19.6
PA6/ABS/SANMA/5% OMMT	4.6	19.3

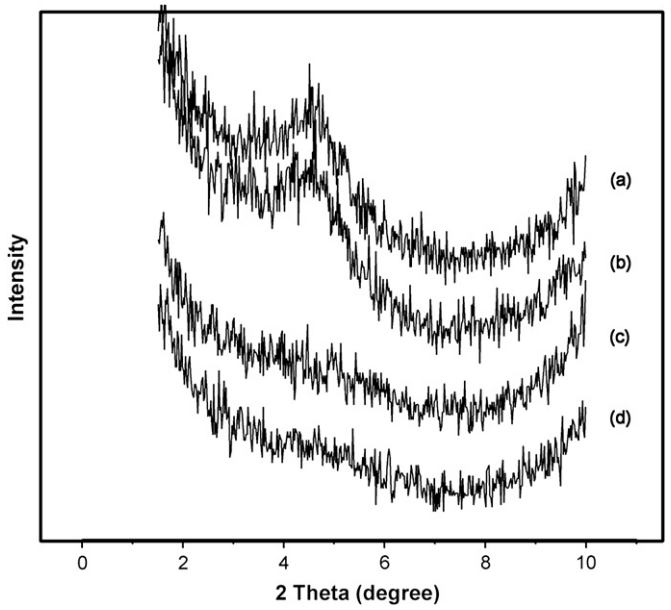

Fig. 2. XRD patterns of (a) PA6/ABS/SANMA/5% OMMT; (b) PA6/ABS/5% OMMT; (c) PA6/SAN/5% OMMT and (d) PA6/SAN/SANMA/5% OMMT.

This implies that the PA6 component helped in the exfoliation process when blended with the SAN. From the XRD investigations on PA6/OMMT nanocomposite we learned that the interaction between OMMT and PA6 is good enough for a complete exfoliation process and a selective localization of the exfoliated clay platelets in the PA6 phase is most likely. Therefore in presence of PA6 the OMMT platelets which are mainly localized in the PA6 phase remain exfoliated in both the PA6/SAN/OMMT and the PA6/SAN/SANMA/OMMT systems. A comparison between the XRD patterns of these two systems indicates that there is no clear effect of the compatibilizer (SANMA) on the dispersion of the OMMT. This implies that the compatibilizer is mainly located at the PA6/SAN interface whereas the OMMT is located in the PA6 phase. Similar results have been reported by other researchers [21,22].

In the ABS based blend nanocomposites (PA6/ABS/OMMT and PA6/ABS/SANMA/OMMT), unlike the SAN based blend nanocomposites, a single diffraction peak at ($2\theta = 4.6^\circ$) corresponding to a d-spacing of 1.93 nm was detected (Fig. 2(a and b)). This indicates that, the PA6/ABS based blends contain OMMT particles the d-spacing of which differs only slightly from that of neat OMMT. It means in presence of ABS there are some non-intercalated OMMT stacks. Since those portions of OMMT which are in the PA6 phase remain exfoliated these stacks should be in the ABS phase. Based on TEM investigations of the ABS/OMMT system it has been reported that the clay particles appear to be attracted to and conform to rubber particle surface. They mainly reside in the SAN matrix phase of ABS with some accumulation at the rubber particle surfaces [28]. In presence of the PA6 phase those accumulated OMMT particles cannot go through intensive shearing during the melt mixing process and hence they remain unchanged. In the ABS/OMMT system in absence of PA6, the applied shearing is good enough for affecting the clays located at the rubber phase to make them intercalated. Therefore the clear difference between the OMMT dispersion states in the SAN based nanocomposites and the ABS based nanocomposites can be attributed to the role of the polybutadiene rubber particles. In the ABS based nanocomposites, a small portion of SAN is replaced by a bulky grafted polymer (SAN-*g*-PB). One should notice that ABS owing to the presence of the polybutadiene rubber domains has much higher viscosity than the SAN [19]. Due to the drastic increase of viscosity and elasticity of the system as a result of the presence of the rubber phase, the state of OMMT dispersion

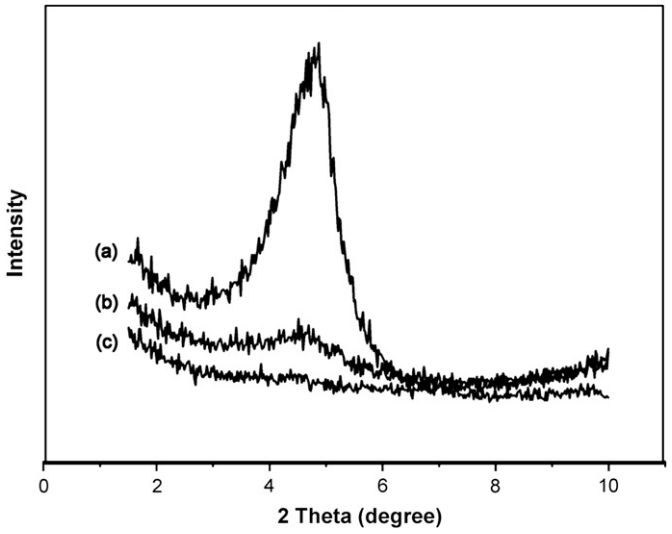

Fig. 3. XRD patterns of (a) neat OMMT; (b) PA6/ABS/SANMA/3% OMMT and (c) PA6/ABS/SANMA/5% OMMT.

changes accordingly. Thus, study of these series of model systems reveals the role of polybutadiene rubber phase and its negative influence on the OMMT dispersion.

On the other hand, the effect of the compatibilizer (SANMA) is found to be negligible in the ABS and SAN based nanocomposites. In both cases it has no significant effect on the level of OMMT dispersion. As stated before, this implies that in these systems OMMT are not located at the PA6/SAN interface for being affected by the compatibilizer. The OMMT is mainly located as exfoliated platelets in the PA6 phase and some OMMT particles in their original non-intercalated states are assumed to be located at the rubber surface. Fig. 3 shows the XRD patterns of PA6/ABS/SANMA nanocomposites with different clay contents. The nanocomposites with 3 and 5 wt% OMMT exhibited X-ray peaks similar to the neat OMMT but with different intensities. The relatively small intensity of the diffraction peak for the nanocomposite with 3 wt% OMMT content might be a hint for an improved distribution at the lower OMMT loading. Although, XRD is very useful for the measurement of *d*-spacing in intercalated systems it may fail at low clay loadings (<5 wt%). Combination of XRD and TEM should be used for a precise result.

3.2. TEM and SEM analysis

3.2.1. PA6/SAN blends and their nanocomposites

Fig. 4(a) shows the morphology of an etched cryofractured surface of PA6/SAN/SANMA blend obtained by SEM, for which PA6 was selectively dissolved. The morphology appears co-continuous. This co-continuous structure is very important from the practical point of view. It is known that blends with co-continuous structures have improved properties as compared with blends with droplet-in matrix morphology [19]. On the other hand, the blends with more refined co-continuous morphologies have better ultimate properties. The OMMT effect on the morphology is shown in Fig. 4(b). As compared to the PA6/SAN/SANMA blend, the addition of 5 wt% OMMT to this system refines the co-continuous structures significantly. This change in behavior can be attributed to the role of exfoliated OMMT platelets in preventing coalescence, due to induced changes in viscosity and elasticity of the system [11,19].

3.2.2. PA6/ABS blends and their nanocomposites

The morphology of the etched cryofractured surface of the PA6/ABS based blends and their nanocomposites are shown in Fig. 5(a–d). Formic acid was used to dissolve the PA6 fraction of the blend revealing the ABS structure. As it is seen from Fig. 5(a), the morphology appears coarse co-continuous. Addition of the SANMA as a compatibilizer causes a significant refinement of the co-continuous structure as evident from the SEM micrographs shown in Fig. 5(b). However, there was a significant change in the blend phase morphology on the addition of a small amount of OMMT. Here, the OMMT seems to have a similar effect as in the SAN based system. Fig. 5(c and d) shows the phase morphology of PA6/ABS and PA6/ABS/SANMA blend nanocomposites containing 5 wt% OMMT. Both blend nanocomposites kept their co-continuous structures, but the phase size decreased on addition of OMMT.

Fig. 6(a and b) shows TEM micrographs of the PA6/SAN/SANMA blend nanocomposite with different magnifications. The white part corresponds to the PA6 phases and the gray part is the SAN phase. The black lines correspond to OMMT layers. Since PA6 and SAN form co-continuous morphology it is hard to distinguish the phases in these TEM images but the OMMT layers and their state of dispersion are clearly visible. As it can be seen the order between the OMMT layers has been lost under the shearing forces imposed by the melt mixing processing and they are mainly in the exfoliated states. This is in agreement with the XRD results. The TEM micrographs of PA6/ABS/SANMA blend nanocomposites containing 5 wt% OMMT are shown in Fig. 6(c and d). The white part corresponds to the PA6 phase and the black particles dispersed in the SAN phase correspond to the butadiene rubber phase. These TEM images reveal an exfoliated structure for the ABS based blend nanocomposite too. But, besides the exfoliated OMMT layers, some thick OMMT stacks are also visible. These OMMT stacks are seen in the SAN phase near the rubber surface and they are responsible for the XRD pattern corresponding to the non-intercalated OMMT seen in the XRD examination of this sample.

3.3. Estimation of interfacial energies of the model systems and prediction of clay localization

The experimental findings about localization of the major part of OMMT particles in the polyamide 6 phase can be supported by considering the interfacial energies of the model systems based on the

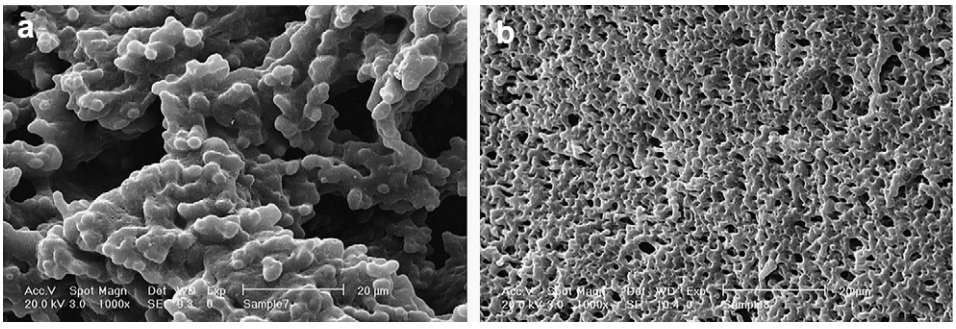

Fig. 4. SEM photomicrographs of (a) PA6/SAN/SANMA and (b) PA6/SAN/SANMA/5% OMMT.

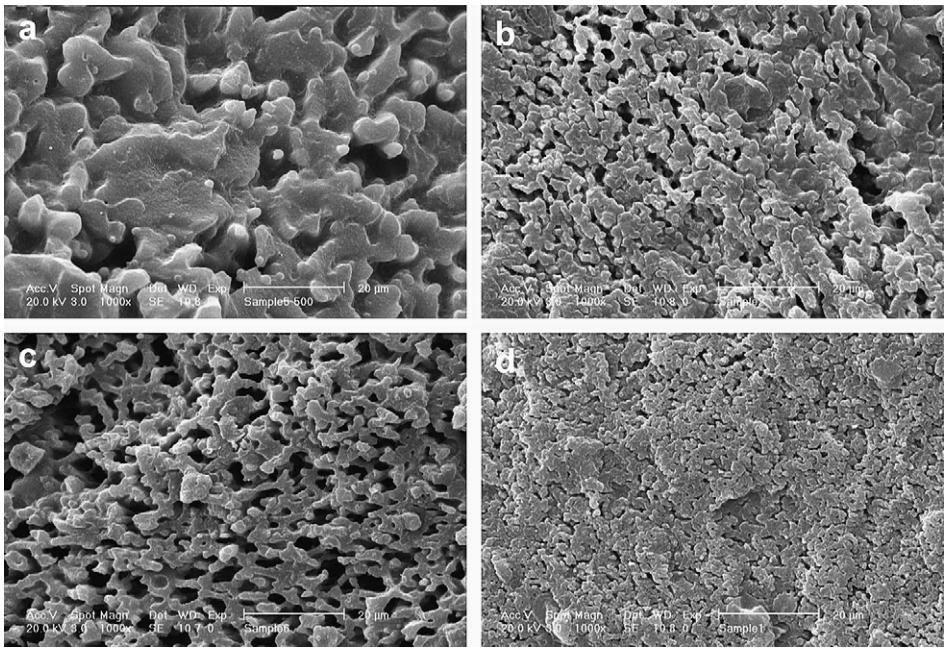

Fig. 5. SEM photomicrographs of (a) PA6/ABS; (b) PA6/ABS/SANMA; (c) PA6/ABS/5% OMMT and (d) PA6/ABS/SANMA/5% OMMT.

fact that the system tries to reach a minimum interfacial energy state.

According to the Young's equation the location of the filler in an equilibrium state can be estimated by calculation of the wetting coefficient ω_a [29]:

$$\omega_a = \frac{\sigma_{OMMT-B} - \sigma_{OMMT-A}}{\sigma_{A-B}} \quad (1)$$

where σ_{OMMT-B} is the interfacial energy between OMMT and polymer component B, σ_{OMMT-A} is the interfacial energy between OMMT and polymer component A and the σ_{A-B} is the interfacial energy between polymer components A and B.

If the wetting coefficient is higher than one, the clays will be located in polymer A, when having values lower than −1, they will be located in polymer B, and if the wetting coefficient is between 1 and −1 the clays are preferentially located at the interface between both polymers. The values of the surface energy of the polymers at the appropriate temperatures were extrapolated from literature values [30–32] and are reported in Table 2. Since the structure of Nanofil 2 is similar to the Nanofil 919 the dispersive and polar free

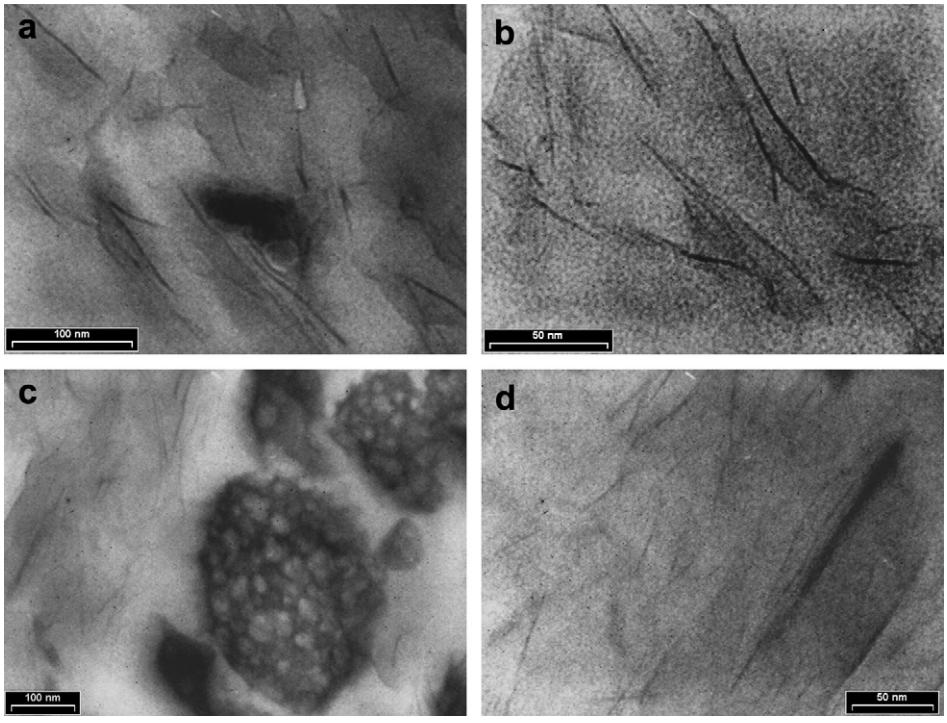

Fig. 6. TEM micrographs of: (a and b) PA6/SAN/SANMA/5% OMMT, and (c and d) PA6/ABS/SANMA/5% OMMT.

Table 2
Total surface free energies and dispersive and polar components of the materials

Materials	Temperature (°C)	Surface energy (mJ/m^2)	Dispersive free surface energy (mJ/m^2)	Polar free surface energy (mJ/m^2)
OMMT [29]	–	29.6	20.0	9.6
PA6	260	30.9[a]	21.6[b]	9.3[b]
SAN	260	23.4[a]	19.9[b]	3.5[b]
ABS	260	24.3[a]	19.7[b]	4.6[b]

[a] Calculated from surface tension values at 20 °C using the temperature coefficient.
[b] Calculated from values given in Refs. [27,28] at 20 °C applying the same temperature coefficient used for calculation of the total surface energies.

surface energies of this kind of OMMT was obtained by extrapolation of the values reported for the Nanofil 919 at different temperatures [32].

The interfacial energy can be calculated from surface energies and their dispersion and polar components. For this purpose mainly two approaches are used, namely the harmonic mean and geometric-mean equations [33].

The harmonic mean equation is commonly used to calculate the interfacial energy between polymer pairs:

$$\sigma_{12} = \sigma_1 + \sigma_2 - 4\left[\frac{\sigma_1^d \sigma_2^d}{\sigma_1^d + \sigma_2^d} + \frac{\sigma_1^p \sigma_2^p}{\sigma_1^p + \sigma_2^p}\right] \quad (2)$$

where σ_1, σ_2 are surface energies of the components 1 and 2, σ_1^d, σ_2^d are disperse part of the surface energies of components 1 and 2, and σ_1^p, σ_2^p are polar part of the surface energies of components 1 and 2.

The geometric-mean equation is described in the literature to be more suitable as compared to the harmonic mean equation for high surface energies [33] (higher than 20 mJ/m^2, according to additional information from [30]):

$$\sigma_{12} = \sigma_1 + \sigma_2 - 2\left(\sqrt{\sigma_1^d \sigma_2^d} + \sqrt{\sigma_1^p \sigma_2^p}\right). \quad (3)$$

These equations were adapted to our systems. The calculated interfacial energies between the polymer pairs and the polymer/OMMT pairs are shown in Table 3.

The values for the wetting coefficients calculated based on Eq. (1) are presented in Table 4. Since the compatibilizer had no influence on the state of OMMT dispersion in these series of model systems, it has not been considered here.

Based on the values obtained for the wetting coefficients the OMMT tends to locate mainly in the PA6 in both nanocomposite systems. Since the values of the wetting coefficients are very close to 1 there are possibilities for localization of small portion of the OMMT in the interface too. In case of ABS based system this small portion of OMMT tends to accumulate near the rubber particle surface at the rubber–SAN interface. These findings are in agreement with the experimental results and they further confirm that the major part of OMMT is located in the PA6 phase. This selective localization affects the properties of the nanocomposites as discussed in the previous section.

Table 3
Interfacial energies as calculated from harmonic and geometric-mean equations

Systems	Temperature (°C)	Interfacial energy according to harmonic mean equation (mJ/m^2)	Interfacial energy according to geometric-mean equation (mJ/m^2)
PA6/ABS	260	1.68	0.86
PA6/SAN	260	2.68	1.41
PA6/OMMT	260	0.07	0.03
SAN/OMMT	260	2.81	1.49
ABS/OMMT	260	1.76	0.91

Table 4
The wetting coefficient for the nanocomposites

System	Wetting coefficient ω_A according to harmonic mean equation (mJ/m^2)	Wetting coefficient ω_A according to geometric mean equation (mJ/m^2)
PA6/SAN/OMMT	+1.03	+1.04
PA6/ABS/OMMT	+1.01	+1.02

3.4. Dynamic mechanical properties

In this section we describe how the OMMT in presence of the other blend components influence the dynamic mechanical properties of the nanocomposites. First we consider the influence of OMMT addition on the DMTA properties of the neat components. The damping (tan δ) and storage modulus (E') of PA6, SAN and ABS without and with 5 wt% OMMT are shown in Fig. 7(a and b) as a function of temperature.

From Fig. 7(a) it is seen that the neat PA6 and its nanocomposite show two peaks at about −55 °C and 44 °C, representing the β relaxation (movement of chain segments and amide groups) and the glass transition temperature (T_g) of its amorphous region, respectively. The neat SAN and its nanocomposite show a single peak at about 114 °C corresponding to the T_g of the styrene component. On the other hand there are also two peaks at −65 °C and 109 °C for ABS system corresponding to the glass transitions of the polybutadiene and SAN components of the ABS, respectively. Comparing the damping peaks of these three neat polymers with their respective nanocomposites one can conclude that the OMMT has no influence or only a very marginal effect on the T_g of all these materials. Although the state of OMMT dispersion was completely different in these series of nanocomposites, the OMMT loading of 5 wt% does not have much influence on the chain segmental mobility. This implies that the free volume in these materials is large enough not to get affected by small amounts of OMMT loading.

However, this small amount of OMMT has a strong influence on the storage modulus of these materials as evident from Fig. 7(b). One can notice that there is a significant enhancement of the modulus for the nanocomposites over the entire temperature range investigated. This enhancement is more pronounced for PA6 especially at temperatures above T_g whereas, SAN and ABS show significant improvements in the modulus up to their glass transition temperatures only. This difference can be attributed to the crystalline nature of PA6 which can retain the structure even up to the melting and to the exfoliated structure of OMMT. ABS has a lower modulus as compared to SAN due to its rubber component but the extent of improvement of modulus is almost the same for these two materials. These two nanocomposites had almost similar intercalated structures as evidenced by the XRD results.

3.4.1. PA6/SAN based blends and blend nanocomposites

The dynamic mechanical properties for the SAN based blend nanocomposites are presented in Fig. 8(a and b). For a better comprehension of the role of OMMT in changing the properties, the DMTA curves for the PA6/OMMT and SAN/OMMT along with the neat components are also embedded in this figure. From Fig. 8(a) one can notice that, similar to the previously discussed case about DMTA properties of the neat components in presence of OMMT, here the OMMT has no influence either or has only a marginal influence on the glass transition temperatures of the PA6 and SAN components of the nanocomposites. Moreover, there is not much difference between the various states of OMMT dispersion (fully exfoliated or intercalated states) as far as their influence on T_g are concerned. One should note that based on the XRD results the SAN based blend nanocomposites with PA6 showed exfoliated morphology whereas, the SAN/OMMT had an intercalated morphology. Even the fully exfoliated PA6/OMMT nanocomposite showed no

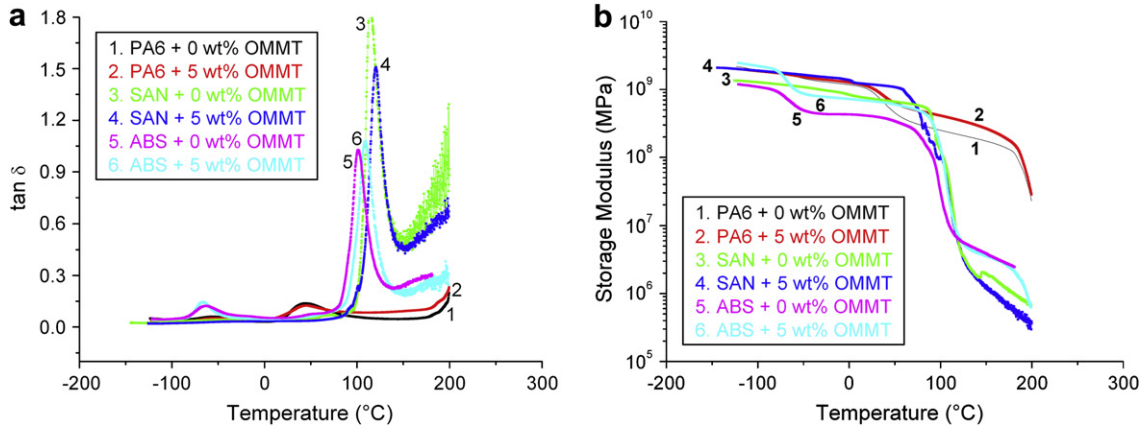

Fig. 7. Dynamic mechanical properties of the neat components and their respective nanocomposites: (a) tan δ versus temperature and (b) storage modulus versus temperature.

changes in T_g compared to neat PA6. Similar results have been reported for other polymer/clay nanocomposites such as ABS/OMMT nanocomposite system with different types of OMMT [34] and also exfoliated and intercalated polyamide–imide/MMT nanocomposites [35].

From Fig. 8(b) one can clearly notice the significant increase in storage modulus and hence stiffening of SAN especially at temperatures above its T_g as a result of blending with PA6 and reinforcement with OMMT in the presence of a compatibilizer. The SAN becomes soft above its T_g (about 114 °C) and starts to flow, but presence of PA6 and OMMT can hold the structure to some extent. The filler–matrix interactions are more pronounced above T_g in which the polymeric chains are not in a confined state. Therefore, when both PA6 and SAN components of the system are above their T_gs the OMMT shows its reinforcing role more effectively. The compatibilized PA6/SAN blend-based nanocomposite containing 5 wt% OMMT, with its co-continuous morphology and exfoliated OMMT structure, has a modulus in between the two main components, i.e. PA6 and SAN with the similar OMMT loading. However, the contribution of OMMT in enhancement of modulus is evident if one compares this multicomponent nanocomposite model system with its counterpart blend system without OMMT. This enhancement in modulus of the blend due to incorporation of OMMT can be attributed to the role of exfoliated OMMT layers in refining the co-continuous morphology as it was evidenced by the SEM analysis.

3.4.2. PA6/ABS based blends and blend nanocomposites

Results of a systematic study on dynamic mechanical properties of ABS-based blend nanocomposites revealing the role of OMMT content and the blend components are presented in Fig. 9(a and b). From Fig. 9(a), it can be seen that, there are three peaks at about −65°C, 44°C and 105°C for all ABS containing systems, representing the β relaxation (movement of chain segments and amide groups) of PA6 which overlaps with the T_g of polybutadiene, the T_g of the amorphous part of PA6 and the T_g of SAN, respectively. The position of all these transition peaks remains almost unchanged and no significant broadening is observed. These findings further confirm the previous results obtained for the other model systems. A marginal decreasing trend is seen in the peak heights, especially at the T_g of SAN at about 114 °C, with increasing OMMT loading from 0 to 5 wt%. This indicates that the OMMT has some tendency towards reducing damping of the system.

Fig. 9(b) shows the storage modulus versus temperature for PA6/ABS based blends and nanocomposites. Here also, one can clearly see the role of OMMT in enhancing the modulus of the system. Increase in OMMT loading leads to further increase in the modulus. This increase in modulus is evident over the entire temperature range investigated but it is more pronounced at high temperatures. As discussed above, there are several factors which can contribute to the enhancement of modulus. The first and the major contribution is exerted from the exfoliated and/or intercalated OMMT layers with their high inherent moduli. Secondly, it is observed that these OMMT layers support the formation of a more refined network-like co-continuous morphology (see Fig. 4(a and b)) which in turn can contribute to the enhancement of the modulus. The role of co-continuous morphology in enhancement of modulus is evident if one compares the modulus of non-reactive PA6/ABS binary blend, having a rough co-continuous morphology, with that of the compatibilized blend system (PA6/ABS/SANMA), having

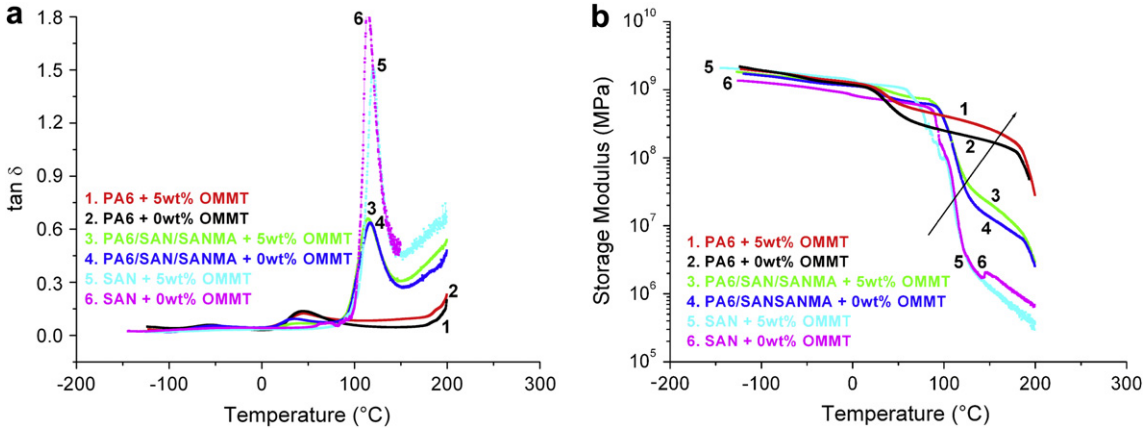

Fig. 8. Dynamic mechanical properties of the SAN based blends and nanocomposites: (a) tan δ versus temperature and (b) storage modulus versus temperature.

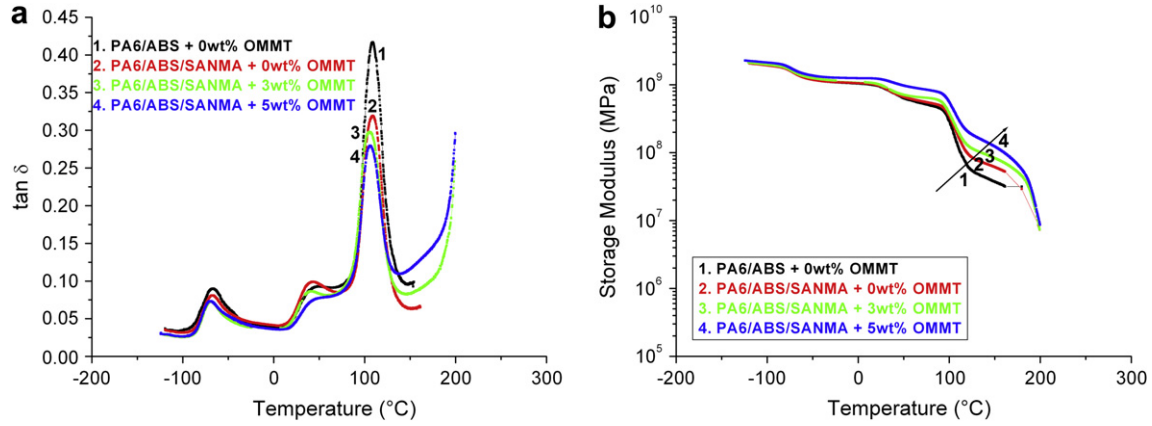

Fig. 9. Dynamic mechanical properties of the ABS based blends and nanocomposites: (a) tan δ versus temperature and (b) storage modulus versus temperature.

comparatively a more refined co-continuous morphology. And lastly, one has to take into account the influence of the polybutadiene rubber domains on to the modulus enhancement with the rise of temperature. This becomes evident if one compares the two sets of nanocomposites with similar compositions but with and without polybutadiene (see Figs. 8(b) and 9(b)).

4. Conclusions

This model study has shown that the behavior of a complicated multicomponent clay-containing polymer blend system can be explained by the help of a structural analysis of a number of simplified model systems. Based on XRD, TEM, SEM and DMTA measurements on various polymer/clay as well as blend/clay systems and a theoretical approach, it was possible to reveal that the most crucial factor in controlling morphology and dispersion is the extent of interaction between OMMT and the polymer matrix. Moreover, the results allowed to approximate the level of dispersion of the OMMT layers in the different phases. It was shown that in PA6, with the highest affinity towards OMMT, a fully exfoliated morphology was formed. The results indicate that these exfoliated clay morphology is also predominant in blends of PA6 with SAN and ABS and that the main part of OMMT is localized in the PA6 phase. However, a distinct difference appeared between PA6/SAN and PA6/ABS blends. In the latter, a significant amount of non-intercalated OMMT was found which was assumed to be accumulated at the rubber particle surface. In the case of PA6/SAN blends the applied mechanical shearing during the melt mixing process seems to be high enough to fully exfoliate the OMMT whereas in PA6/ABS blends full exfoliation failed. It is assumed that in PA6/ABS blends a certain part of the OMMT particles remain in their original non-intercalated states at the rubber particle surface since the main shear stress during mixing is assimilated from the PA6 phase. Interestingly, in the absence of PA6, both the systems with and without rubber showed a similar partially intercalated morphology. This model study also revealed that the compatibilizer (SANMA) does not play an important role in dispersion of OMMT in the blends.

Further, it could be shown that the presence of OMMT in the blends did not change the general appearance of their co-continuous structures, but, refined the structures and led to mechanical stiffening as indicated by the DMA results. Moreover, the selective localization of the exfoliated OMMT layers in the PA6 phase, increased the modulus of the blends especially at temperatures above T_g of ABS. This was attributed to the role of crystalline regions of PA6 in maintaining the structure till it melts. Incorporation of OMMT in all the model systems did not have any influence on the glass transition temperature of the materials. However, it led to a small reduction in damping especially with increasing the OMMT loading.

This kind of systematic study has proven very useful in understanding and interpreting the structural changes in multicomponent clay-containing nanocomposites for establishing a good correlation between the structures and resulting properties.

References

[1] Unal H, Mimaroglu A, Alkan M. Polym Int 2004;53(1):56–60.
[2] Takahara A, Magome T, Kajiyama T. J Polym Sci Part B Polym Phys 1994;32(5):839–46.
[3] Dibenedetto AT. Mater Sci Eng A 2001;302(1):74–82.
[4] Wang Y, Zhang Q, Fu Q. Macromol Rapid Commun 2003;24(3):231–5.
[5] Khatua BB, Lee DJ, Kim HY, Kim JK. Macromolecules 2004;37(7):2454–9.
[6] Li Y, Shimizu H. Polymer 2004;45(22):7381–8.
[7] Gelfer MY, Song HH, Liu L, Hsiao BS, Chu B, Rafailovich MY, et al. J Polym Sci Part B Polym Phys 2003;41(1):44–54.
[8] Yurekli K, Karim A, Amis EJ, Krishnamoorti R. Macromolecules 2003;36(19):7256–67.
[9] Lim SK, Kim JW, Chin I, Kwon YK, Choi HJ. Chem Mater 2002;14(5):1989–94.
[10] Yurekli K, Karim A, Amis EJ, Krishnamoorti R. Macromolecules 2004;37(2):507–15.
[11] Kim HB, Choi JS, Lee CH, Lim ST, Jhon MS, Choi HY. Eur Polym J 2005;41(4):679–85.
[12] Jafari SH, Pötschke P, Stephan M, Pompe G, Warth H, Alberts H. J Appl Polym Sci 2002;84(14):2753–9.
[13] Henton DE, Mang MN, U.S. Patent 5,089,557; 1992.
[14] Weber M, Heckmann W, Goeldel A. Macromol Symp 2006;233(1):1–10.
[15] Liu XI, La Mantia F, Scaffaro R. J Appl Polym Sci 2002;86(2):449–55.
[16] Kitayama N, Keskkula H, Paul DR. Polymer 2000;41(22):8041–52.
[17] Kitayama N, Keskkula H, Paul DR. Polymer 2000;41(22):8053–60.
[18] Kitayama N, Keskkula H, Paul DR. Polymer 2001;42(8):3751–9.
[19] Jafari SH, Pötschke P, Stephan M, Warth H, Alberts H. Polymer 2002;43(25):6985–92.
[20] Özkoc G, Bayram G, Bayramli E. Polymer 2004;45(26):8957–66.
[21] Lai SM, Liao YC, Chen TW. J Appl Polym Sci 2006;100(2):1364–71.
[22] Lai SM, Liao YC, Li HC. Eur Polym J 2007;43(5):1660–71.
[23] Li YJ, Shimizu H. Macromol Rapid Commun 2005;26(9):710–5.
[24] Özkoc G, Bayram G, Quaedflieg M. J Appl Polym Sci 2008;107:3058–70.
[25] Özkoc G, Bayram G, Tiesnitsch. Polym Compos 2008;29(4):345–56.
[26] Bose S, Bhattacharyya AR, Kodgire PV, Misra A, Pötschke P. Polymer 2007;48(1):356–62.
[27] Meincke O, Kaempfer D, Weickmann H, Friedrich C, Vathauer M, Warth H. Polymer 2004;45(3):739–48.
[28] Stretz HA, Paul DR, Cassidy PE. Polymer 2005;46:3818–30.
[29] Sumita M, Sakata K, Asai S, Miyasaka K, Nakagawa H. Polym Bull 1991;25(2):265–71.
[30] <http://www.surface-tension.de/solid-surface-energy.htm>; 2008 [accessed 4.01.08].
[31] <http://www.topanalytica.com/files/94/3surface_free_energy_of_ABS_plastic.pdf> 2008 [accessed 4.01.08].
[32] Picard E, Gauthier H, Gérard JF, Espuche E. J Colloid Interface Sci 2007;307(2):364–76.
[33] Wu S. Polymer interface and adhesion. New York: Marcel Dekker Inc; 1982.
[34] Ranade A, D'Souza NA, Gnade B. Polymer 2002;43(13):3759–66.
[35] Patino-Soto AP, Sanchez-Valdes S, Ramos-DeValle LF. Macromol Mater Eng 2007;292(3):302–9.